NASA Technical Memorandum 107274
ICOMP–96–6; AIAA–96–3145

Rocket-Based Combined Cycle Engine Technology Development—Inlet CFD Validation and Application

J.R. DeBonis
Lewis Research Center
Cleveland, Ohio

and

S. Yungster
Institute for Computational Mechanics in Propulsion
Cleveland, Ohio

Prepared for the
32nd Joint Propulsion Conference
cosponsored by AIAA, ASME, SAE, and ASEE
Lake Buena Vista, Florida, July 1–3, 1996

National Aeronautics and
Space Administration

Rocket-Based Combined Cycle Engine Technology Development - Inlet CFD Validation and Application

J. R. DeBonis
NASA Lewis Research Center
Cleveland, Ohio

and

S. Yungster
Institute for Computational Mechanics in Propulsion
Cleveland, Ohio

Abstract

A CFD methodology has been developed for inlet analyses of Rocket-Based Combined Cycle (RBCC) Engines. A full Navier-Stokes analysis code, NPARC, was used in conjunction with pre- and post-processing tools to obtain a complete description of the flow field and integrated inlet performance. This methodology was developed and validated using results from a subscale test of the inlet to a RBCC "Strut-Jet" engine performed in the NASA Lewis 1x1 ft. supersonic wind tunnel. Results obtained from this study include analyses at flight Mach numbers of 5 and 6 for super-critical operating conditions. These results showed excellent agreement with experimental data. The analysis tools were also used to obtain pre-test performance and operability predictions for the RBCC demonstrator engine planned for testing in the NASA Lewis Hypersonic Test Facility. This analysis calculated the baseline fuel-off internal force of the engine which is needed to determine the net thrust with fuel on.

Nomenclature

A_0	freestream area of captured streamtube
A_i	inlet geometric projected area
F	force
M	Mach number
p	pressure
S	surface
V	velocity
ρ	density
τ_w	wall shear stress

subscripts

closed	closed or solid surface
exp	experimentally obtained force
ext	external force
int	internal force
mom	momentum balance force
off	fuel off condition
on	fuel on condition
open	open or permeable surface
p/sf	pressure/skin friction force
p	pitot
viscous	viscous force
x	axial distance
∞	freestream

Introduction

Currently, interest in hypersonic propulsion systems is on the rise. These systems have a variety of applications including missile, reconnaissance and single stage to orbit vehicles. The propulsion system must operate efficiently throughout the flight regime from takeoff to hypersonic cruise. To accomplish this, combined cycle engines are

being studied. Because different propulsion cycles operate more efficiently at different flight conditions, these engines combine two or more different propulsion cycles into one integrated system for better performance. One such propulsion system being developed at the NASA Lewis Research Center is the Rocket-Based Combined Cycle Engine (RBCC)[1]. This engine integrates a high specific impulse low thrust-to-weight airbreathing engine with a low specific impulse high thrust-to-weight rocket. From takeoff to Mach 2.5 the engine operates as an air-augmented rocket. At Mach 2.5 the rockets are turned off and the engine is transitioned to a dual-mode ramjet. Beyond Mach 8 the rocket would be turned back on.

One RBCC engine concept under development at Lewis is the "Strut-Jet" concept (Fig. 1). This work is a joint effort between NASA Lewis, the United States Air Force, Gencorp Aerojet, GASL and Lockheed Martin. This engine contains two struts in the inlet to provide compression. The struts divide the flow into three separate flow paths. The rockets are embedded in the base of the struts. The fuel injectors needed for the ramjet mode are also housed in the struts.

A demonstration of this engine concept at Mach 6 and 7 flight conditions is scheduled for NASA Lewis' Hypersonic Tunnel Facility (HTF)[2]. Critical to the success of this demonstration is the performance of the inlet. It must: provide sufficient pressure recovery over the entire Mach number range, demonstrate reasonable starting and unstart characteristics, provide a mass distribution adequate for combustion and operate with a low internal drag. Because of the inlet's importance, a significant effort has been focused on providing a good understanding of its behavior. This effort included a subscale experiment in the NASA Lewis 1x1 ft. supersonic wind tunnel[3] and the development of a computational fluid dynamics (CFD) capability for RBCC inlet analysis. This paper focuses on the development, validation and application of the CFD capability for RBCC combined cycle inlets.

Computational Approach

The methodology developed for the Strut-Jet analyses utilized a combination of government developed codes (grid generator, flow solver and post-processors) already in use at NASA Lewis. The codes' capabilities and the existing experience base were the reasons for their selection.

Geometry Definition and Grid Generation

The Strut-Jet geometry can be defined as a series of flat planes with no curvature or irregularities of the surfaces. The coordinates which defined these planes were taken from a set of engineering drawings for the subscale inlet model. A short FORTRAN code was written to generate a set of points which lay on the strut-jet surfaces. This surface database was then input into the grid generator.

The grid generator used for this work was GRIDGEN version 9.6[4]. It is an interactive graphical interface driven code which runs on UNIX workstations. The grid was subdivided into several domains in order to simplify grid generation. In order to keep the number of mesh points defining the strut to a reasonable level, the break lines defining the changes in strut width were not explicitly modeled. However, all grid points were constrained to lie on the database surface. This was deemed to be a reasonable compromise between geometric accuracy and computational efficiency.

Two grids were used for this study (Fig. 2 and 3). The first grid models the subscale inlet experiment and was used for analysis at the super-critical conditions. The second grid models the demonstrator engine flow-path for the HTF test. It is based on the first grid, but the last block was modified to represent the exhaust nozzle on the demo-engine. Both grids model one-half of the symmetric inlet flow path, including the pre-compression plate, diverter, center duct, side duct and combustor. Table 1 gives detailed information on the grids generated for this study.

Flow Solution

Code - The NPARC code[5] was used as the flow solver. It is a general purpose computational fluid dynamics code which is widely used in government, industry and academia for fluid flow simulations, particularly of aircraft propulsion systems components.

NPARC solves the Reynolds averaged Navier-Stokes equations in strong conservation law form using the Beam-Warming approximate factorization algorithm[6]. Spatial discretization is performed using a central difference scheme. Jameson-style artificial dissipation is added for stability and to smooth shock oscillations and odd-even grid point decoupling[7]. The code uses a perfect gas equation of state.

NPARC is very flexible in handling computational grids. The code allows the user to specify a boundary condition on any portion of any grid surface. This allows a complex geometry to be handled using one grid block. It is also capable of using grids subdivided into multiple grid blocks. The grid points may or may not be contiguous across the block interface. In the case of a noncontiguous interface, the code uses a trilinear interpolation scheme to pass data through the boundary.

The code has several options for modeling turbulence varying from algebraic (zero transport equations) to one and two equation models. The Chien low-Reynolds number k-ε model[8] was used for this work. It has been shown to give good results for a wide range of flow problems.

Boundary Conditions.- A fixed supersonic inflow was specified upstream of the pre-compression plate. Flow conditions were extrapolated to the boundaries at regions of supersonic outflow, including the diverter and exit planes. Solid boundaries were treated as no slip adiabatic walls. Symmetry about the inlet centerline was assumed and a slip wall was specified on this plane.

Post Processing

The flow solution was processed to determine, wall static pressure distributions, massflow distributions, pitot pressure distributions and internal drag. A separate FORTRAN code was written to perform these calculations. Pressure distributions, on the cowl and body along the centerline, and on the sidewall are output for comparison to experimental data. For the sidewall pressure distribution, the location of the experimental data did not lie on a computational grid line. Therefore, the computational pressures had to be interpolated onto the experimental locations for comparison. Mass continuity was checked by integrating the massflow over each axial grid plane through the duct. Pitot pressure distributions at the strut base were used to compute massflow, distortion and pressure recovery for comparison to experiment. The computational pressures were interpolated onto the experimental rake positions in order to eliminate any differences that would be caused by lower resolution of the experimental data. The experimental data reduction program was then used to process the data for comparison.

The internal drag of the inlet was computed using a control volume method[9]. The momentum equation written in control volume form is

$$\oiint_S (\rho V \cdot dS)V = -\oiint_S p dS + F_{viscous}$$

where,

$$F_{viscous} = \oiint_S \tau_w dS$$

The control volume for the Strut-Jet is shown in Figure 4. It is drawn such that no portion of the control volume passes through a solid surface. The control volume can be separated into the open or permeable surfaces and the closed or solid surfaces. For the closed surfaces, the momentum flux terms are zero. For permeable surfaces the viscous forces are zero. This yields the following equation.

$$\iint_{S_{open}} (\rho V \cdot dS)V + \iint_{S_{open}} pdS = -\iint_{S_{closed}} pdS + F_{viscous}$$

The right hand side of this equation represents the forces on the solid surfaces and is the internal force generated on the inlet. It is equivalent to the integral of the net rate flow of momentum and pressure over the open control volume surfaces as represented by the left hand side of the equation. Therefore the internal force on the inlet can be calculated by either a pressure skin friction integration or a momentum flux integration.

$$F_{p/sf} = -\iint_{S_{closed}} pdS + F_{viscous}$$

$$F_{mom} = \iint_{S_{open}} (\rho V \cdot dS)V + \iint_{S_{open}} pdS$$

Typically, accurate calculation of skin friction from a CFD solution is difficult, due to grid skewness at the wall and boundary layer resolution. The momentum flux integration offers a simpler less computationally intensive way to determine the drag force. Both methods were examined in this study to determine the best method for application to this flow problem.

Experimental Programs

Subscale Inlet Test

Results from the subscale inlet test were used for the code validation portion of this study. This test was performed in the NASA Lewis 1x1 ft. supersonic wind tunnel. It is a one-pass continuous flow facility that can provide Mach numbers from 1.3 to 6.0 in the test section. These Mach numbers are achieved by changing two-dimensional fixed geometry nozzle blocks. The air is heated to prevent condensation and liquification of the flow. The test program ran at Mach 4.0, 5.0, 5.5, and 6.0. CFD comparisons were made for the Mach 5.0 and Mach 6.0 conditions.

The geometry is a 40 percent scale model of the demonstrator engine inlet. The model uses a pre-compression plate to generate the initial shock wave. The model was mounted 0.4 in. below this plate in order to divert the pre-compression plate boundary layer. Static pressure taps were located on the model centerline on both the cowl and body surfaces and on the model sidewalls. A traversing rake of 12 pitot pressure tubes (3 in each side duct and 6 in the center duct) was located at the base of struts. The rake took measurements at 20 equally spaced intervals. A wedged shaped massflow plug was used to simulate combustion back-pressure. The plug simulates several back pressured conditions between super-critical (no back pressure) and critical (near inlet unstart). The CFD comparisons presented here were made at super-critical conditions. Code validation at back pressured conditions is ongoing.

Demonstrator Engine Test

The complete Strut-Jet engine will be demonstrated at NASA Lewis' Hypersonic Tunnel Facility (HTF) in the Summer of 1996. HTF, located at Lewis' Plum Brook Station, is a blow-down non-vitiated free-jet facility capable of providing true air composition for testing up to Mach 7 flight conditions.

In this experiment the engine will be tested in both the air-augmented rocket and ramjet modes. The rockets operate on monomethyl hydrazine (MMH) and inhibited red fuming nitric acid (IRFNA). In ramjet mode the engine is fueled by Liquid JP-10 injected from the struts. The JP-10 is piloted by MMH-IRFNA pilots. HTF will be operated at test section Mach numbers of 5 and 6, with enthalpy levels corresponding to Mach 6 and 7. This is done to simulate some vehicle forebody compression. The engine will be instrumented with static pressure taps and a limited number of thermocouples and dynamic pressure transducers. The engine will be mounted in the test section on a force balance. The balance will measure the total force on the engine including internal and external components.

$$F_{exp} = F_{int} + F_{ext}$$

From this force data one can obtain the change in internal force on the engine between fuel-off and fuel-on conditions, assuming that the external forces are not affected by fueling the engine.

$$\Delta F = F_{on} - F_{off}$$
$$= (F_{\text{int}_{on}} + F_{ext}) - (F_{\text{int}_{off}} + F_{ext})$$
$$= F_{\text{int}_{on}} - F_{\text{int}_{off}}$$

However because the external drag of the engine cannot be separated out of the fuel-on measurement, the true thrust produced by the engine cannot be obtained directly from the experiment. The CFD analysis for this test program focused on obtaining the internal force on the engine at fuel-off conditions. By adding the change in thrust between fuel-on and fuel-off conditions to the fuel-off internal force obtained by CFD, an estimate of the net internal engine thrust can be made.

$$F_{\text{int}_{on}} = F_{\text{int}_{off}} + \Delta F$$

Results

Code Validation, Subscale Inlet Calculations

Code validation was done by analyzing the subscale inlet geometry and comparing the results to experimental data. The inlet was analyzed at super-critical conditions for freestream Mach numbers of 5 and 6. The Mach 5 calculation was run at a freestream static pressure of 25.50 psf and a freestream static temperature of 118.5 R. The Mach 6 calculation was run at a freestream static pressure of 14.98 psf and a freestream static temperature of 93.13 R. Near critical analyses at Mach 5 and 6 are underway, but were not completed at the time of this report.

Mach 5, Super-Critical.- A contour plot of static pressure on the inlet's centerline plane (Fig. 5a) clearly shows a series of strong oblique shocks initiated by the pre-compression plate. A series of shock waves in the transverse direction is created by the strut leading edge and are evidenced by the near vertical pressure contours on the forward portion of the inlet. Mach contours (Fig. 5b) indicate a large region of low speed flow along the body side of the inlet. This low energy flow is initially caused by a boundary layer separation induced by the transverse shock. The reflections of the cowl shock onto the body side creates a series of adverse pressure gradients which continue to enlarge the low speed region.

Figure 6 compares the predicted static pressure distributions to the experimental data for the cowl, body and sidewall surfaces. Agreement for the cowl and body pressures is very good. On the cowl centerline the large fore and aft pressure rises are due to the cowl shock and its subsequent reflection. The transverse shock from the strut creates the small pressure rise at x=18 inches. On the body centerline pressure rises at x=21 inches and x=26.5 inches are generated by the reflected cowl shock. The code overpredicts the pressures along the sidewall. This could be due an over-prediction of the side ducts' massflow, caused by the fact that the analysis assumed no spillage around the sidewalls.

A comparison of pitot pressure distributions at the base of the struts is shown in Figure 7. Overall the CFD predicts lower levels of pressure throughout the duct. The predicted shapes of the contours are qualitatively correct.

Results of the internal drag calculation are shown in Table 2. The data shown is for the computational domain which is one half of the actual inlet. Forces for each surface of the integration are listed for both methods. For the momentum calculation positive values represent momentum flowing out the control volume and negative values represent momentum flowing in. For the pressure/skin friction calculation positive values represent thrust and negative values represent drag. At this condition the methods agree within 7 percent.

Mach 6, Super-Critical.- Qualitatively the Mach 6 results are very similar to the Mach 5 results. The contour plot of static pressure on the inlet's centerline plane (Fig. 8a) again shows the cowl and transverse shocks and their reflections. Mach contours (Fig. 8b) show the

large region of low speed flow along the body side of the inlet.

Figure 9 compares the predicted static pressure distributions to the experimental data for the cowl, body and sidewall surfaces. Agreement for the cowl and body pressures is very good. On the cowl centerline the large fore and aft pressure rises are due to the cowl shock and its subsequent reflection. The transverse shock from the strut creates the small pressure rise at x=18 inches. On the body centerline pressure rises due to the reflected cowl shock, x=22 inches, is better resolved than at the Mach 5 condition. The sidewall pressure distribution is overpredicted and the discrepancy is slightly larger for this case.

A comparison of pitot pressure distributions at the base of the struts is shown in Figure 10. Agreement is good for the side ducts. In the center duct near the body side the region of low energy flow is predicted very well. Near the cowl surface, the analysis predicts a large region of high pressure low distortion flow whereas the experiment measured a lower pressure more distorted flowfield.

Results of the internal drag calculation are shown in Table 3. At this condition the methods agree within 1.5 percent. At both Mach numbers calculation of skin friction was difficult and time consuming. Problems arose in determining the vector normal to the wall in skewed areas of the grid. Because of this and the fact that agreement between the force calculations was good, the momentum flux integration was used for the remainder of the calculations to determine the internal drag.

Code Application, Demonstrator Engine Calculations

Once satisfactory results were obtained on the subscale inlet model the code was then applied to the demonstrator engine geometry in order to obtain the fuel-off internal drag to support the experimental program. There are two significant differences between subscale inlet and demonstrator engine calculations. First the constant area combustor section of the subscale test was replaced with the engine's exhaust nozzle. Second, true high temperature flight conditions consistent with the engine test were used instead of the cold temperatures of the subscale experiment. At the fuel-off (no combustion) condition there is no back-pressure on the inlet. Therefore these results are comparable to the super-critical subscale inlet results. Both the Mach 5.2 and Mach 6 calculations were run at a freestream static pressure of 89.1374 psf and a freestream static temperature of 514.8 R.

Mach 5.2 - Contour plots of pressure and Mach number (Fig. 11) indicate that the flowfield is very similar to the cold subscale results. The shock system appears to be the same as the subscale case. The boundary layers on the pre-compression plate and in the inlet appear to be thicker. The Mach contours in the exhaust nozzle show that the flow there is distorted. Pressure distributions on the cowl and body centerlines (Fig. 12) have the same shape as the subscale inlet experiment. This implies that the shock system is the same. Any differences in the pressure levels between the subscale inlet and the demonstrator engine can be attributed to viscous effects.

Fuel-off internal drag calculated using the momentum flux integral is show in Table 4. As in the subscale results the values are for the computational domain which represents one half of the inlet.

Mach 6 - Contour plots of pressure and Mach number (Fig. 13) again indicate that the flowfield is very similar to the cold subscale results. The boundary layers on the pre-compression plate and in the inlet appear to be thicker. The Mach contours in the exhaust nozzle show that the flow there is distorted. Again, the pressure distributions on the cowl and body centerlines (Fig. 14) have the same shape as the subscale results. At identical freestream Mach numbers the demonstrator engine result has noticeably lower pressure levels than the subscale result. This is further evidence of a stronger viscous interaction in the demonstrator engine.

Fuel-off internal drag calculated using the momentum flux integral is show in Table 4. The decreased drag at higher Mach number is consistent with the subscale results.

Inlet Mass Capture

Using the computed massflow from both the subscale inlet and demonstrator engine calculations the inlet massflow ratio was determined. Figure 15 shows these results in relation to the theoretical results. The theoretical results were computed using two-dimensional inviscid streamlines. They are shown for both the engine flow and the total flow which includes the flow which passes through the diverter. The theory neglects the compression due to the struts upstream of the cowl lip. This compression creates additional flow turning which will decrease the freestream capture area. It also neglects the boundary layer on the pre-compression plate. The theory predicts that the pre-compression shock is on the cowl lip at Mach 5 and all the flow is captured without spillage. The diverter reduces the amount of flow into the inlet and the amount of diverted flow increases with Mach number. The CFD results indicate that spillage flow continues to exist beyond Mach 5 because the capture area continues to increase with Mach number. This is due to the additional compression of the struts. The demonstrator engine results show a higher capture ratio than the subscale results, and than the theory at Mach 6. This may be accounted for by the large boundary layer on the pre-compression plate which reduces the amount of flow that can enter the diverter.

Concluding Remarks

A CFD methodology for analyzing inlets for Rocket-Based Combined Cycle propulsion systems was developed. This methodology was put in place to support an upcoming demonstration of an RBCC engine concept, the Strut-Jet. The resulting system was validated against data obtained from a subscale test of the Strut-Jet inlet. Very good agreement between the analysis and experimental data was obtained for surface static pressure distributions, and pitot pressure profiles. A means for determining the internal drag of the system was also developed. Two methods a momentum flux integral and a pressure/skin friction integration were examined. Both methods yielded similar results for the subscale inlet. However, the momentum flux integral proved to be less computationally intensive and easier to implement. The validated analysis tools were then applied to the demonstrator engine and internal drag forces were obtained. These forces will be used in the upcoming test to compute the net thrust of the engine.

References

1. Escher, W.J.D., Hyde, E.H. and Anderson, D.M., "A User's Primer for Comparative Assessments of All-Rocket and Rocket-Based Combined-Cycle Propulsion Systems for Advanced Earth-to-Orbit Space Transport Applications," AIAA 95-2474, July 1995.

2. Thomas, S.R., Trefny C.J. and Pack W.D., "Operating Capability and Current Status of the Reactivated NASA Lewis Research Center Hypersonic Tunnel Facility," AIAA 95-6146, NASA TM 106808, April 1995.

3. Fernandez, R., Trefny, C.J., Thomas, S.R. and Bulman, M., "Parametric Data from a Wind Tunnel Test on a Rocket Based Combined Cycle Engine Inlet," NASA TM 107181, July 1996.

4. Steinbrenner, J.P. and Chawner, J.R., "Automatic Structured Grid Generation Using Gridgen (Some Restrictions Apply)," NASA CP 3291, Surface Modeling, Grid Generation, and Related Issues in CFD Solutions, NASA Lewis Research Center, Cleveland, Ohio, May 1995.

5. Cooper, K., "NPARC 2.0 - Features and Capabilities," AIAA 95-2609, July 1995.

6. Beam, R. and Warming, R.F., "An Implicit Finite Difference Algorithm for Hyperbolic Systems in Conservation Law Form," J. Comp. Phys., vol. 22, no. 1, September 1976, pp. 87-110.

7. Jameson, A., Schmidt, W. and Turkel, E., "Numerical Solutions of the Euler Equations by Finite Volume Method for Solving the Euler and Navier-Stokes Equations for High Speed Flows," AIAA 81-1259, June 1981.

8. Chien, K.-Y., "Predictions of Channel and Boundary-Layer Flows With a Low-Reynolds-Number Turbulence Model," AIAA Journal, vol. 20, no. 1, January 1982, pp. 33-38.

9. Voland, R.T., "Methods for Determining the Internal Thrust of Scramjet Engine Modules from Experimental Data," AIAA 90-2340, July 1990.

Block	Description	Dimensions	Total
1	leading edge, center	22 x 76 x 30	50,160
2	center duct	111 x 57 x 30	189,810
3	side duct	111 x 57 x 51	322,677
4	leading edge, side	22 x 76 x 52	86,944
5	pre-compression plate	59 x 95 x 80	448,400
6	combustor	51 x 57 x 104	302,328
Total			1,400,319

a) Subscale inlet

Block	Description	Dimensions	Total
1	leading edge, center	22 x 76 x 30	50,160
2	center duct	111 x 57 x 30	189,810
3	side duct	111 x 57 x 51	322,677
4	leading edge, side	22 x 76 x 52	86,944
5	pre-compression plate	59 x 95 x 80	448,400
6	combustor/nozzle	74 x 57 x 104	438,672
Total			1,536,663

b) Demonstrator engine,

Table 1. Computational grid dimensions

Mometum		Pressure/Skin Friction		
Surface	Momentum (lbs)	Surface	Pressure (lbs)	Skin Friction (lbs)
Inflow	-36.8044	Body	-1.9772	-0.5371
Spillage	3.6303	Cowl	0.0000	-0.3973
Outflow	29.0882	Strut	0.7459	-1.3593
		Sidewall	0.0000	-0.7129
		Base	0.4306	0.0000
Total	-4.0859	Total	-3.8073	

Table 2. Force summary, subscale inlet, M_∞=5

Mometum		Pressure/Skin Friction		
Surface	Momentum (lbs)	Surface	Pressure (lbs)	Skin Friction (lbs)
Inflow	-32.3999	Body	-1.3563	-0.4740
Spillage	0.8108	Cowl	0.0000	-0.3226
Outflow	28.3773	Strut	0.4575	-1.1703
		Sidewall	0.0000	-0.6499
		Base	0.2566	0.0000
Total	-3.2118	Total	-3.2590	

Table 3. Force summary, subscale inlet, M_∞=6

	Mach 5.2	Mach 6.0
Surface	Momentum (lbs)	Momentum (lbs)
Inflow	-910.7325	-1275.2389
Spillage	62.5419	65.9264
Outflow	807.0910	1189.3104
Total	-41.0996	-20.0021

Table 4. Force summary, demonstrator engine

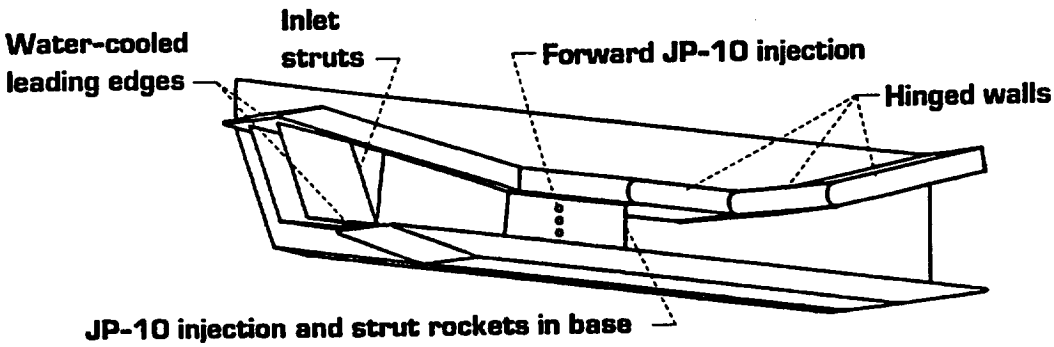

Figure 1. Schematic of the Strut-Jet engine concept.

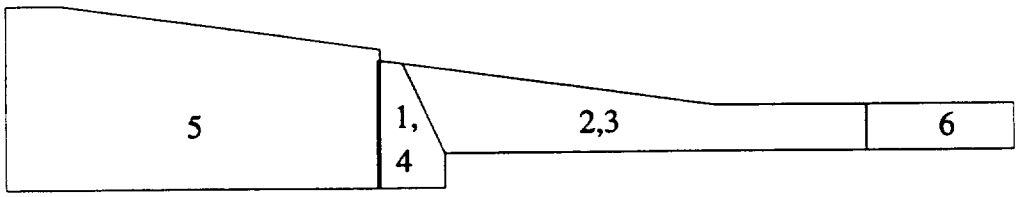

a) Block structure; plane of symmetry

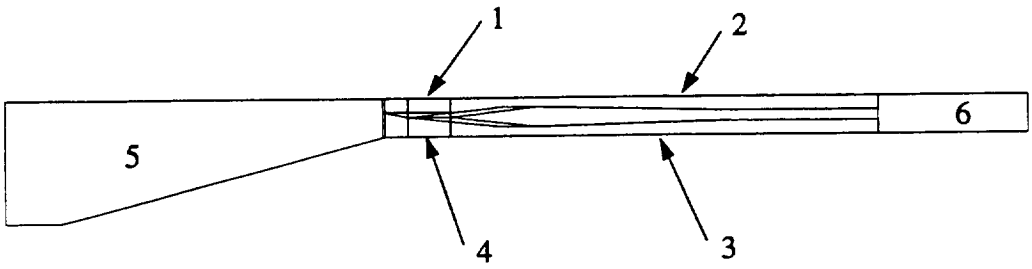

b) Block structure; body surface

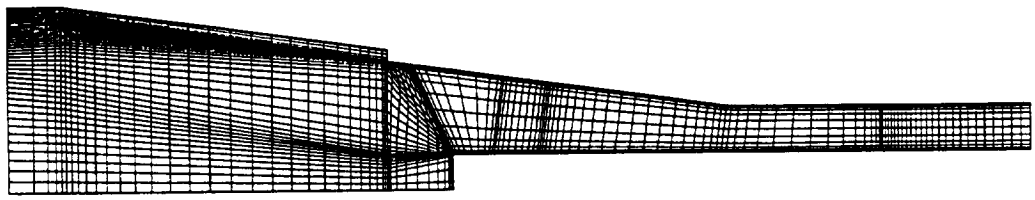

c) grid points; plane of symmetry

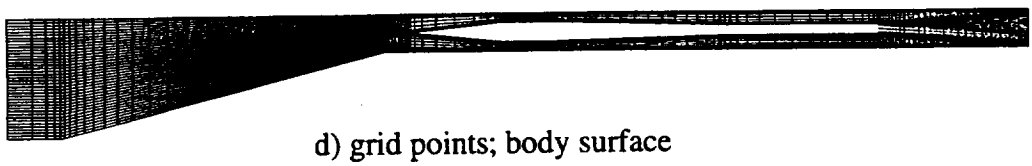

d) grid points; body surface

Figure 2. Subscale inlet block structure and grid used for super-critical calculations

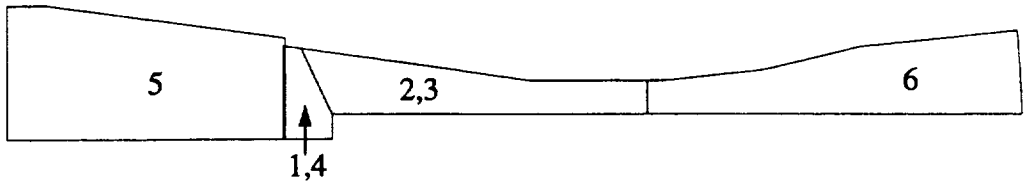

a) Block structure; plane of symmetry

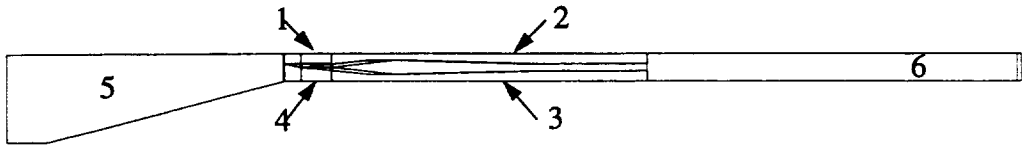

b) Block structure; body surface

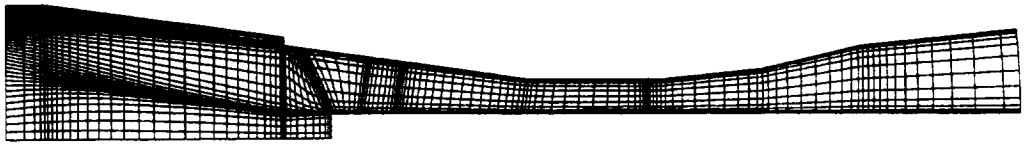

c) grid points; plane of symmetry

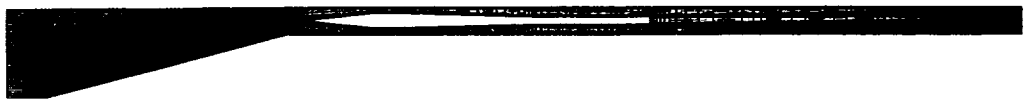

d) grid points; body surface

Figure 3. Demonstrator engine inlet block structure and grid

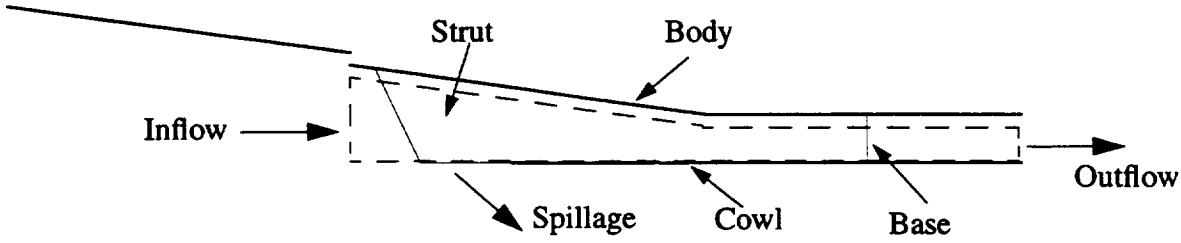

Figure 4. Control volume used in internal drag calculation (sidewall removed).

a) pressure contours

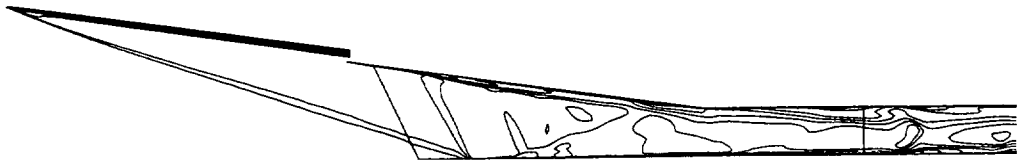

b) Mach number contours

Figure 5. Subscale inlet pressure (p/p_∞) and Mach number contours for $M_\infty = 5$ super-critical flow. Contour ranges: a) 1.4-32.2; b) 0.2-5.0.

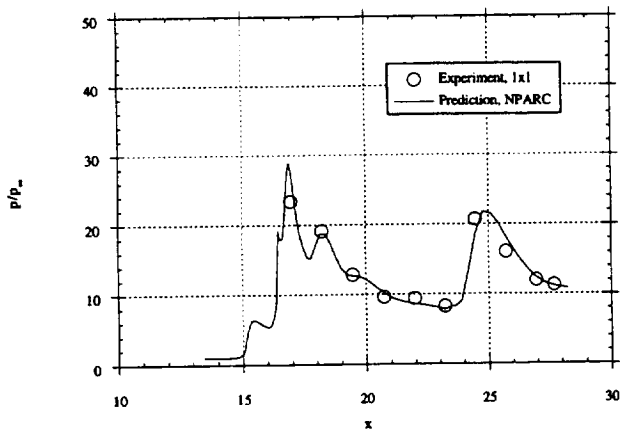

a) Cowl centerline

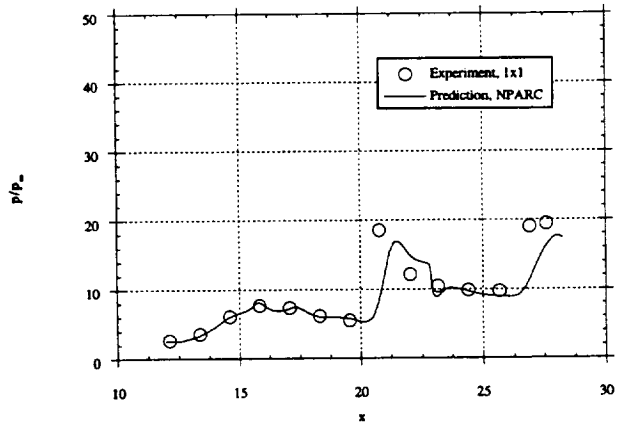

b) Body centerline

Figure 6. Subscale inlet pressure distribution; $M_\infty = 5$ super-critical flow.

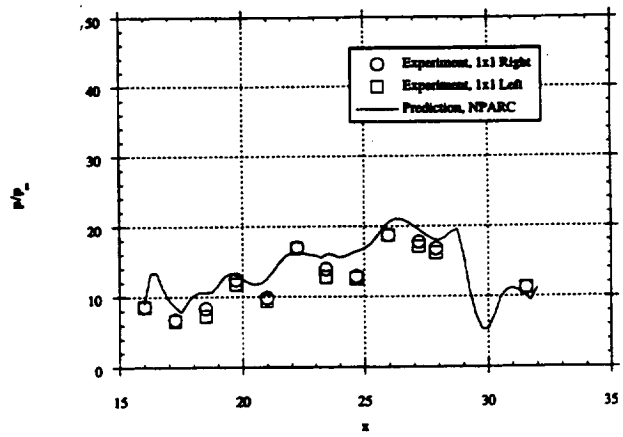

c) Sidewall

Figure 6. Continued.

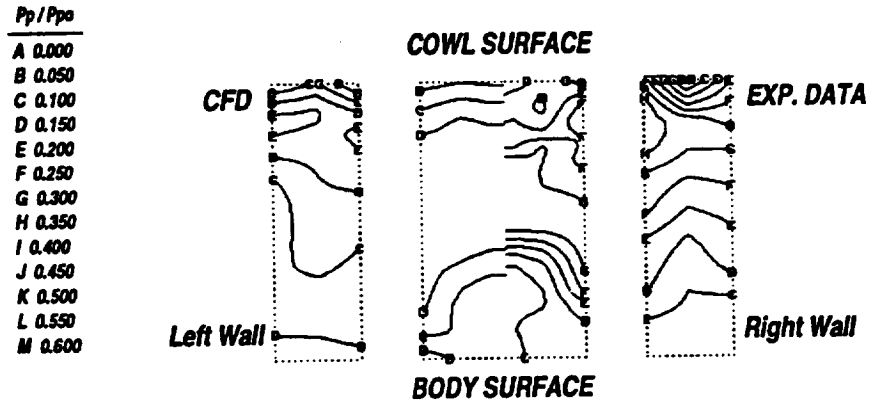

Figure 7. Comparison of subscale inlet Pitot pressure contours at strut base. $M_\infty = 5$, super-critical flow.

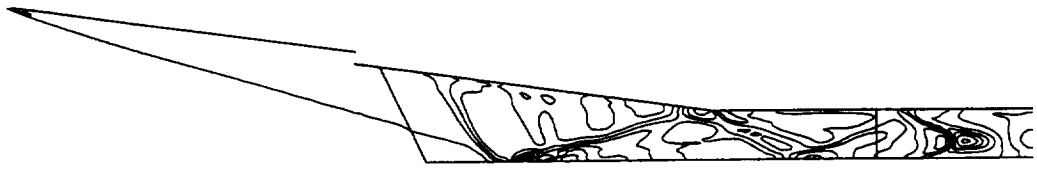

a) pressure contours

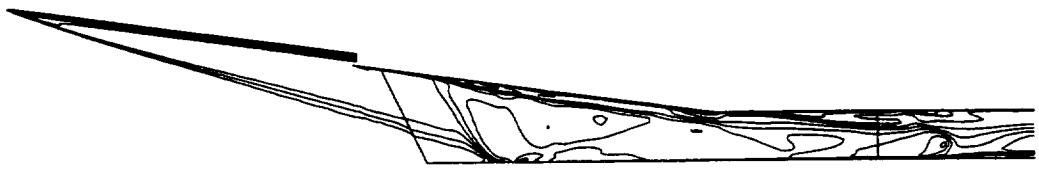

b) Mach number contours

Figure 8. Subscale inlet pressure (p/p_∞) and Mach number contours for $M_\infty = 6$ super-critical flow. Contour ranges: a) 1.4-49.0; b) 0.2-6.2.

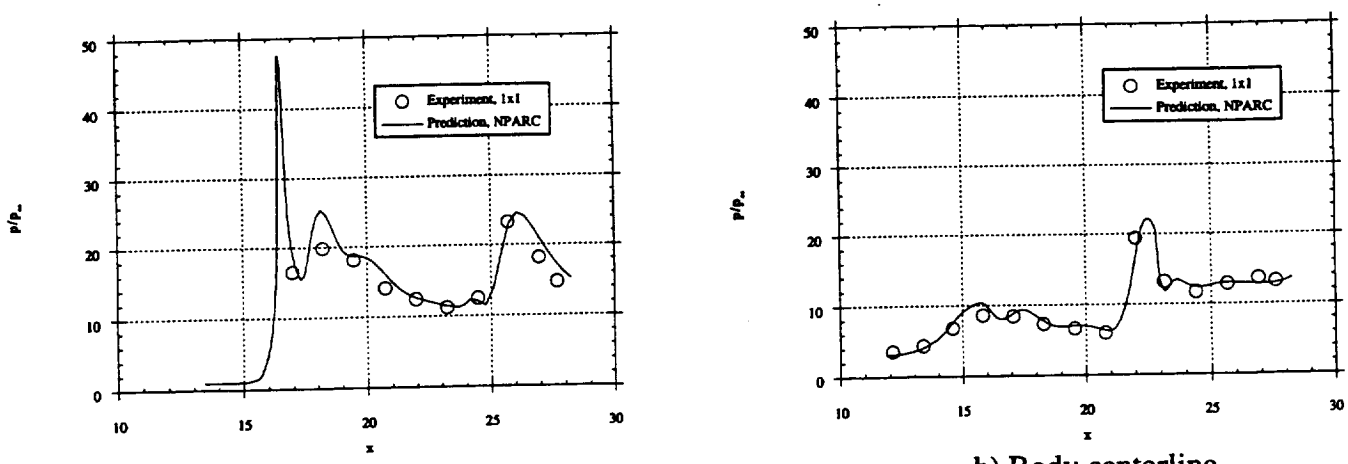

a) Cowl centerline

b) Body centerline

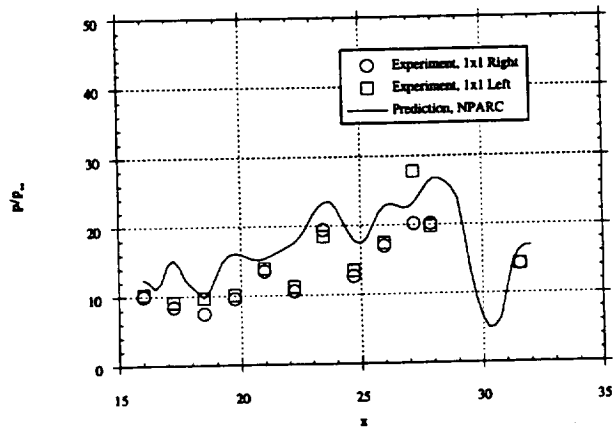

c) Sidewall

Figure 9. Subscale inlet pressure distribution; $M_\infty = 6$ super-critical flow.

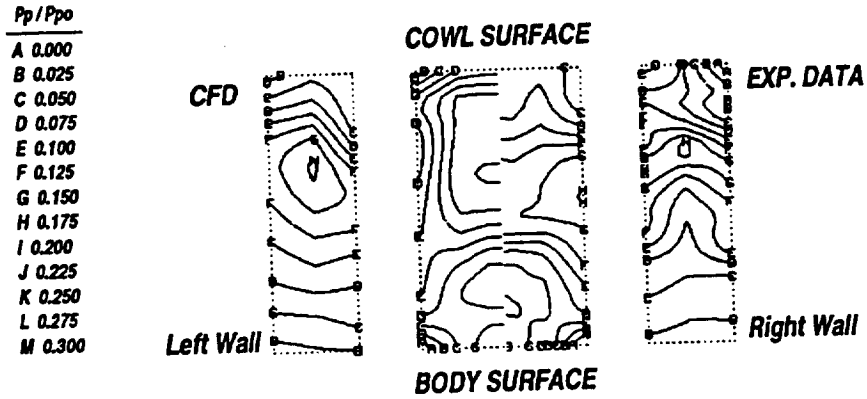

Figure 10. Comparison of subscale inlet Pitot pressure contours at strut base. $M_\infty = 6$, super-critical flow.

a) pressure contours

b) Mach number contours

Figure 11. Demonstrator engine pressure (p/p_∞) and Mach number contours for $M_\infty = 5.2$. Contour ranges: a) 0.0-32.0; b) 0.0-5.2.

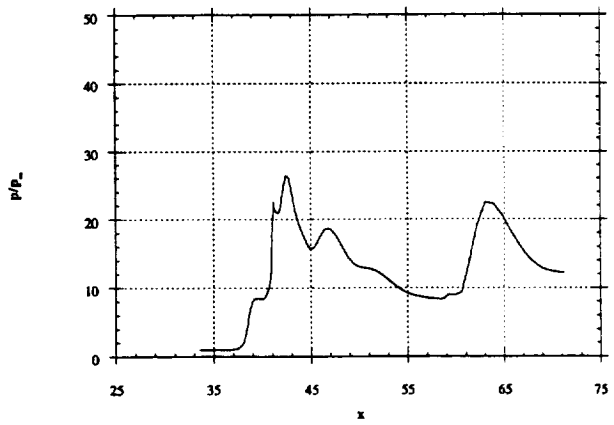

a) Cowl centerline

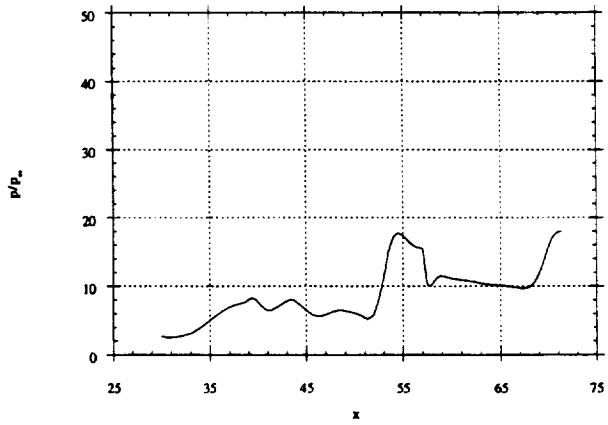

b) Body centerline

Figure 12. Demonstrator engine pressure distribution; $M_\infty = 5.2$.

a) pressure contours

b) Mach number contours

Figure 13. Demonstrator engine pressure (p/p_∞) and Mach number contours for $M_\infty = 6.0$. Contour ranges: a) 0.0-53.0; b) 0.0-6.0.

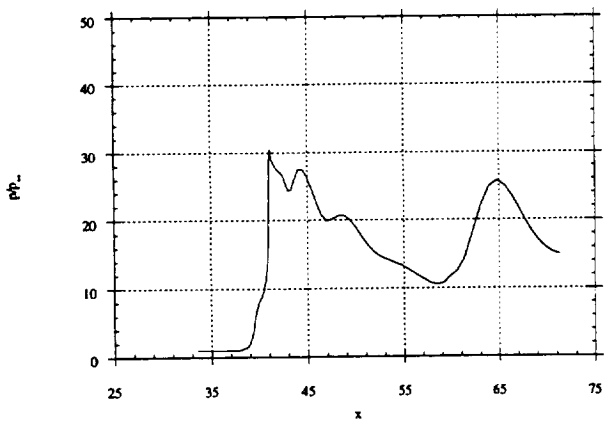

a) Cowl centerline

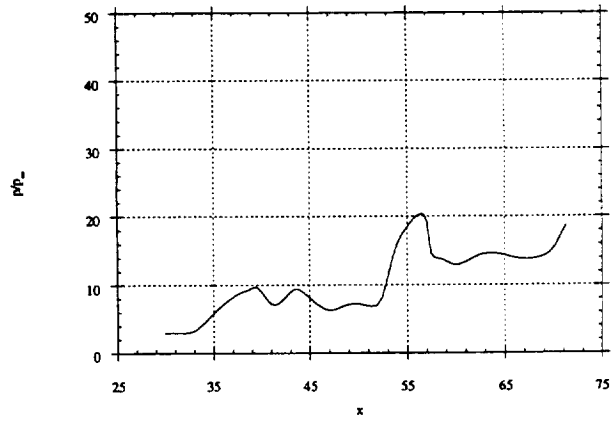

b) Body centerline

Figure 14. Demonstrator engine pressure distribution; $M_\infty = 6.0$.

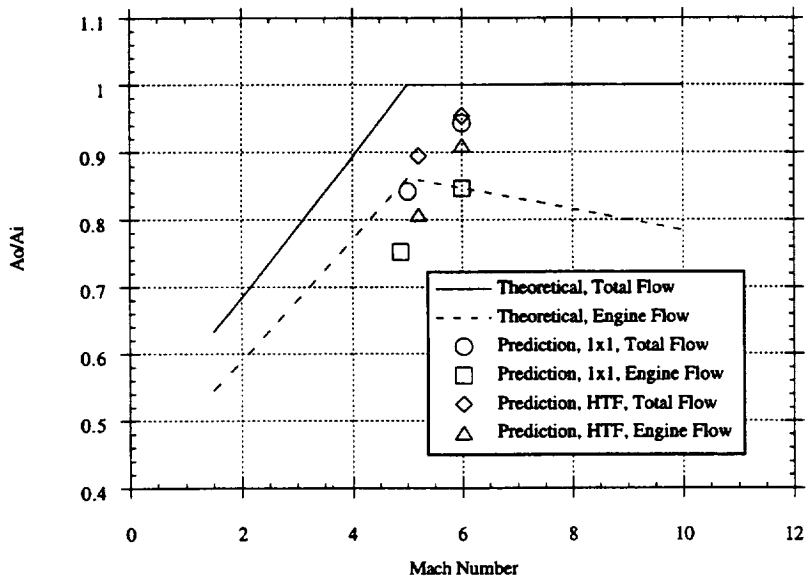

Figure 15. Inlet capture area ratio

REPORT DOCUMENTATION PAGE

Form Approved
OMB No. 0704-0188

1. AGENCY USE ONLY (*Leave blank*)	2. REPORT DATE	3. REPORT TYPE AND DATES COVERED
	June 1996	Technical Memorandum

4. TITLE AND SUBTITLE

Rocket-Based Combined Cycle Engine Technology Development—Inlet CFD Validation and Application

5. FUNDING NUMBERS

WU–505–70–62

6. AUTHOR(S)

J.R. DeBonis and S. Yungster

7. PERFORMING ORGANIZATION NAME(S) AND ADDRESS(ES)

National Aeronautics and Space Administration
Lewis Research Center
Cleveland, Ohio 44135–3191

8. PERFORMING ORGANIZATION REPORT NUMBER

E–10342

9. SPONSORING/MONITORING AGENCY NAME(S) AND ADDRESS(ES)

National Aeronautics and Space Administration
Washington, D.C. 20546–0001

10. SPONSORING/MONITORING AGENCY REPORT NUMBER

NASA TM–107274
ICOMP–96–6
AIAA–96–3145

11. SUPPLEMENTARY NOTES

Prepared for the 32nd Joint Propulsion Conference cosponsored by AIAA, ASME, SAE, and ASEE, Lake Buena Vista, Florida, July 1–3, 1996. J.R. DeBonis, NASA Lewis Research Center, and S. Yungster, Institute for Computational Mechanics in Propulsion, NASA Lewis Research Center, Cleveland, Ohio (work performed under NASA Cooperative Agreement NCC3–370). ICOMP Program Director, Louis A. Povinelli, organization code 2600, (216) 433–5818.

12a. DISTRIBUTION/AVAILABILITY STATEMENT

Unclassified - Unlimited
Subject Categories 07, 02, and 20

This publication is available from the NASA Center for AeroSpace Information, (301) 621–0390.

12b. DISTRIBUTION CODE

13. ABSTRACT (*Maximum 200 words*)

A CFD methodology has been developed for inlet analyses of Rocket-Based Combined Cycle (RBCC) Engines. A full Navier-Stokes analysis code, NPARC, was used in conjunction with pre- and post-processing tools to obtain a complete description of the flow field and integrated inlet performance. This methodology was developed and validated using results from a subscale test of the inlet to a RBCC "Strut-Jet" engine performed in the NASA Lewis 1x1 ft. supersonic wind tunnel. Results obtained from this study include analyses at flight Mach numbers of 5 and 6 for super-critical operating conditions. These results showed excellent agreement with experimental data. The analysis tools were also used to obtain pre-test performance and operability predictions for the RBCC demonstrator engine planned for testing in the NASA Lewis Hypersonic Test Facility. This analysis calculated the baseline fuel-off internal force of the engine which is needed to determine the net thrust with fuel on.

14. SUBJECT TERMS

Rocket based combine cycle; Computational fluid dynamics; Inlet

15. NUMBER OF PAGES

20

16. PRICE CODE

A03

17. SECURITY CLASSIFICATION OF REPORT	18. SECURITY CLASSIFICATION OF THIS PAGE	19. SECURITY CLASSIFICATION OF ABSTRACT	20. LIMITATION OF ABSTRACT
Unclassified	Unclassified	Unclassified	

National Aeronautics and
Space Administration

Lewis Research Center
Cleveland, OH 44135-3191